Article

Verification of Two-Way Time Transfer Accuracy Through a Closed-Loop Topology of Inter-Satellite and Satellite-Ground Optical Links

Manuele Dassié [1,2,*], Grzegorz Michalak [1] and Gabriele Giorgi [1]

[1] German Aerospace Center (DLR), Münchener Strasse 20, 82234 Wessling, Germany;
[2] Technische Universität Berlin (TUB), Strasse des 17. Juni 135, 10623 Berlin, Germany;
* Correspondence: manuele.dassie@dlr.de; Tel.: +49 8153 28 4963

Abstract: The exploitation of Optical Inter-Satellite Links (OISLs) has the potential to provide significant benefits to GNSSs, offering clock synchronization via highly accurate time transfer, precise ranging, robustness against jamming and spoofing, high data rates, and freedom from signal frequency regulations. As with any new technology, it is crucial to conduct in-space experiments to demonstrate the capabilities of OISLs before widespread adoption. In this work, we present preliminary analyses of an in-orbit demonstrator concept, which is being designed under the name Optical Synchronized Time And Ranging (OpSTAR). It involves two satellites in a trailing configuration, each equipped with two laser terminals. On the ground, two co-located Optical Ground Stations (OGSs) are operated. Whenever both satellites are simultaneously visible from the OGSs, an OISL and two additional Optical Satellite-to-Ground Links (OSGLs) are established, forming a closed "measurement loop" between the two satellites and the two ground stations. We present a functional model for OISL and OSGL pseudorange observables. A cross-link clock observable is formed by differencing two one-way pseudoranges, from which a relative clock offset estimate is obtained. First, we analyze how modelling errors on differential delays in Two-Way Time Transfer (TWTT) – relativistic effects, atmospheric delays, hardware delays, and satellite dynamics during the exchange – impact the estimation accuracy. Next, we study the impact of individual error contributions to the overall zero-sum chain of clock offset estimates across the closed-loop. Results show that errors due to mis-modeling of relativistic effects, satellite dynamics and clock instability are negligible, while hardware and atmospheric delays require accurate calibrations to achieve TWTT at picosecond-level accuracy.

Keywords: Optical inter-satellite link; Two-way time transfer; Synchronization;

Received:
Revised:
Accepted:
Published:

Citation: Dassié, M.; Michalak, G.; Giorgi, G. Verification of Two-Way Time Transfer Accuracy Through a Closed-Loop Topology of Inter-Satellite and Satellite-Ground Optical Links. *Journal Not Specified* **2025**, *1*, 0. https://doi.org/

1. Introduction

The development of terminals for Optical Inter-Satellite Links (OISLs) has progressed significantly over the past decades. Initial ground-to-space tests of time transfer via non-coherent optical links demonstrated synchronization performances in the range of hundreds of picoseconds, for example within the Laser Time Transfer technology on Beidou satellites (around 300 picoseconds precision) [1] and the Time Transfer by Laser Link (T2L2) with Jason-2 (below 100 picoseconds accuracy) [2]. More recently, the German Aerospace Center (DLR) has designed and implemented coherent optical transceivers to precisely retrieve the time-of-arrival of well-defined events of transmission and reception, showing sub-picosecond time transfer precision in a laboratory set-up and in a 10 kilometers long-range free-space optical demonstrator [3].

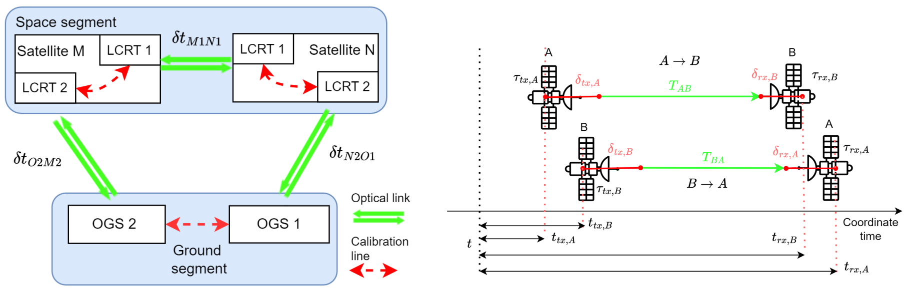

(**a**) (**b**)

Figure 1. The left plot **(a)** shows the OpSTAR in-orbit demonstrator concept and the closed-loop scenario. The right one **(b)** illustrates a two-way exchange of signals and relevant quantities: transmission and reception epochs, hardware delays and signal travel times.

The Optical Synchronized Time And Ranging (OpSTAR) mission proposed by the European Space Agency is intended as an in-orbit testbed for payloads enabling bi-directional optical links for time transfer and ranging. It consists of two satellites flying in a trailing configuration on the same orbital plane, carrying two optical terminals each. Part of the ground segment consists of two co-located and inter-connected Optical Ground Stations (OGSs), see Figure 1a. The two satellites establish an OISL and, when co-visible from OGSs, also establish Optical Satellite-to-Ground Links (OSGLs). All optical terminals employed enable comparing clocks between the two satellites (via the OISL) and between each satellite and the linked OGS (via the two OSGLs). By calibrating the two OGSs and the two terminals onboard the same satellite, i.e. their clock offsets are accurately surveyed, the chain of differential clock measurements in a close measurement loop can be used to assess the accuracy of the synchronization layer offered by the optical links.

2. Optical link observables: functional model

Let us consider two linked endpoints A and B, located in an Earth-centered inertial frame at positions $\mathbf{r}_A(t)$ and $\mathbf{r}_B(t)$, respectively. Here t represents a coordinate time scale – hereafter referred to as system time – assumed to be aligned with a reference terrestrial time scale such as UTC or the Galileo System Time. At each endpoint a free-running clock defines a local time scale, denoted with $\tau_A(t)$ and $\tau_B(t)$. The raw observable in this context is the pseudorange, derived from optical signals exchanged between the endpoints. Direct spread spectrum sequences, such as e.g. pseudo-random noise codes, are modulated on an optical frequency carrier and regularly emitted according to a predefined grid of instants on each endpoint's local time scale, e.g. every second or integer fraction of a second. Consider a signal exchange from endpoint A to B (cf. Figure 1b). Endpoint A transmits a signal timestamped at local time $\tau_{tx,A}$. This signal undergoes hardware delays – due to the propagation in the electronic components, cables, and fibers – denoted with $\delta_{tx,A}(t_{tx,A})$ before reaching the terminal's Optical Phase Center (OPC). The term $t_{tx,A}$ is the coordinate time instant associated to the emission timestamp, satisfying $t_{tx,A} = \tau_{tx,A} - \delta_{rel,A}(t_{tx,A}) - \delta t_A(t_{tx,A})$ where $\delta_{rel,A}(t_{tx,A})$ represents the relativistic offset and $\delta t_A(t_{tx,A})$ is the clock offset of endpoint A with respect to the system time. The signal then propagates in free space with a travel time of T_{AB} to the OPC at endpoint B, where is then affected by additive hardware delays, denoted with $\delta_{rx,B}(t_{tx,A} + \delta_{tx,A}(t_{tx,A}) + T_{AB})$. Finally, the reception is time-stamped at local time $\tau_{rx,B}$, associated to the coordinate time $t_{rx,B} = t_{tx,A} + \delta_{tx,A}(t_{tx,A}) + T_{AB} + \delta_{rx,B}(t_{tx,A} + \delta_{tx,A}(t_{tx,A}) + T_{AB})$.

The travel time T_{AB} is the sum of three delay terms: $T_{AB} = T_{AB,Eucl}(t_{tx,A}, T_{AB}) + \delta T_{AB,atmo}(t_{tx,A}, T_{AB}) + \delta T_{AB,Shapiro}(t_{tx,A}, T_{AB})$. The term $T_{AB,Eucl}(t_{tx,A}, T_{AB})$ is the signal propagation delay in a flat spacetime:

$$T_{AB,Eucl}(t_{tx,A}, T_{AB}) = \frac{\|\mathbf{r}_B(t_{tx,A} + \delta_{tx,A}(t_{tx,A}) + T_{AB}) - \mathbf{r}_A(t_{tx,A} + \delta_{tx,A}(t_{tx,A}))\|}{c} \tag{1}$$

The term $\delta T_{AB,atmo}(t_{tx,A}, T_{AB})$ denotes atmospheric delays, usually experienced in OSGLs. The term $\delta T_{AB,Shapiro}(t_{tx,A}, T_{AB})$ is the Shapiro delay due to gravity-induced space-time curvature. The difference between the local transmit and receive timestamps, scaled by the speed of light c, provides a pseudorange observable, modelled as:

$$\begin{aligned}
\rho_{AB}(t_{tx,A}, T_{AB}) = c(\tau_{rx,B} - \tau_{tx,A}) & \\
= cT_{AB,Eucl}(t_{tx,A}, T_{AB}) & \quad \text{(travel time)} \\
+ c\delta T_{AB,atmo}(t_{tx,A}, T_{AB}) & \quad \text{(atmospheric delay)} \\
+ c\delta T_{AB,Shapiro}(t_{tx,A}, T_{AB}) & \quad \text{(Shapiro delay)} \\
+ c(\delta_{rx,B}(t_{rx,B}) + \delta_{tx,A}(t_{tx,A})) & \quad \text{(hardware delays)} \\
+ c(\delta t_B(t_{rx,B}) - \delta t_A(t_{tx,A})) & \quad \text{(differential clock offset)} \\
+ c(\delta_{rel,B}(t_{rx,B}) - \delta_{rel,A}(t_{tx,A})) & \quad \text{(differential relativistic delay)} \\
+ \varepsilon_{AB} & \quad \text{(measurement error)}
\end{aligned} \tag{2}$$

In this model, the contribute of additional differential relativistic delays (other than the Shapiro propagation effect) are accounted in the relativistic delay term.We assume additive white noise with variance σ^2: $\varepsilon_{AB} \sim \mathcal{N}(0, \sigma^2)$.

The pseudorange model for the propagation from B to A is specular to model (2). The coordinate transmission times $t_{tx,A}$ and $t_{tx,B}$ are typically not simultaneous. This means that each term in the pseudorange equation is calculated at distinct time instants. The objective of time transfer is to estimate the clock offset between linked pairs at an arbitrarily chosen common coordinate epoch t (also represented in Figure 1b). Assuming that t is close to both transmission times $t_{tx,A}$ and $t_{tx,B}$, the pseudorange can be expressed as sum of quantities evaluated at time t via a Taylor expansion in the form $f(t_x) \approx f(t) + \dot{f}(t)(t_x - t)$ for each term, where t_x is any argument that the term may have in (2). This leads to the following approximation:

$$\begin{aligned}
\rho_{AB}(t, t_{tx,A}, T_{AB}) \approx\ & R_{AB}(t) + c\delta t_{AB}(t) + c\delta_{rel,AB}(t) + c\delta_{hw,AB}(t) \\
& + \mathbf{N}_{AB}(t) \cdot \mathbf{v}_B(t)(t_{tx,A} + \delta_{tx,A}(t) + T_{AB} - t) \\
& - \mathbf{N}_{AB}(t) \cdot \mathbf{v}_A(t)(t_{tx,A} + \delta_{tx,A}(t) - t) \\
& + c\delta\dot{t}_B(t)(t_{rx,B} - t) - c\delta\dot{t}_A(t)(t_{tx,A} - t) \\
& + c\dot{\delta}_{rel,B}(t)(t_{rx,B} - t) - c\dot{\delta}_{rel,A}(t)(t_{tx,A} - t) \\
& + c\dot{\delta}_{rx,B}(t)(t_{rx,B} - t) + c\dot{\delta}_{tx,A}(t)(t_{tx,A} - t) \\
& + c\delta T_{AB,atmo}(t_{tx,A}, T_{AB}) + c\delta T_{AB,Shapiro}(t_{tx,A}, T_{AB}) + \varepsilon_{AB}
\end{aligned} \tag{3}$$

where $R_{AB}(t) = \|\mathbf{r}_B(t) - \mathbf{r}_A(t)\|$, $\mathbf{N}_{AB}(t) = (\mathbf{r}_B(t) - \mathbf{r}_A(t))/R_{AB}(t)$ and $\mathbf{v}_{A/B}(t) = \dot{\mathbf{r}}_{A/B}(t)$. We used the notation $x_{AB}(t) = x_B(t) - x_A(t)$ for $x_{A/B}(t) \in \{\delta t_{A/B}, (t), \delta_{rel,A/B}(t)\}$ and $\delta_{hw,AB}(t) = (\delta_{tx,A}(t) + \delta_{rx,B}(t))$. In this expansion we assume that the hardware delays are sufficiently stable to be considered constant when they appear in the argument of a function, i.e. they satisfy $f(t + \delta_{tx/rx,A/B}(t_{tx/rx,A/B})) \approx f(t + \delta_{tx/rx,A/B}(t))$. The terms related to the Shapiro and atmospheric delays have not been expanded as they will be treated separately. The analogous expression for the pseudo-range B to A, $\rho_{BA}(t, t_{tx,B}, T_{BA})$, can be obtained by swapping subscripts A and B in (3).

The two one-way pseudorange observables can be combined to form a Cross-link Clock Observable (CCO) [4]:

$$\Delta^{CCO}_{A\rightleftarrows B} = \frac{\rho_{AB}(t_{tx,A}, T_{AB}) - \rho_{BA}(t_{tx,B}, T_{BA})}{2c} \tag{4}$$

Using the linearized expressions (3) for both one-way pseudoranges and noting that $\mathbf{N}_{BA}(t) = -\mathbf{N}_{AB}(t)$, $\delta t_{BA}(t) = -\delta t_{AB}(t)$, $\delta t_{rel,BA}(t) = -\delta t_{rel,AB}(t)$ and $R_{BA}(t) = R_{AB}(t)$, the inter-satellite range $R_{AB}(t)$ cancels-out in the clock observable. The model for the CCO becomes:

$$\begin{aligned} \Delta^{CCO}_{A\rightleftarrows B} \approx \delta t_{AB}(t) + \delta_{rel,AB}(t) + \Delta^{hw}_{A\rightleftarrows B} + \Delta^{atmo}_{A\rightleftarrows B} + \Delta^{Shapiro}_{A\rightleftarrows B} \\ + \Delta^{Dynamics}_{A\rightleftarrows B} + \Delta^{clkRate}_{A\rightleftarrows B} + \Delta^{relRate}_{A\rightleftarrows B} + \Delta^{hwRate}_{A\rightleftarrows B} + \varepsilon \end{aligned} \tag{5}$$

where:

- $\Delta^{hw}_{A\rightleftarrows B} = \frac{\delta_{hw,AB}(t) - \delta_{hw,BA}(t)}{2}$;
- $\Delta^{atmo}_{A\rightleftarrows B} = \frac{\delta T_{AB,atmo}(t_{tx,A}, T_{AB}) - \delta T_{BA,atmo}(t_{tx,B}, T_{BA})}{2}$;
- $\Delta^{Shapiro}_{A\rightleftarrows B} = \frac{\delta T_{AB,Shapiro}(t_{tx,A}, T_{AB}) - \delta T_{BA,Shapiro}(t_{tx,B}, T_{BA})}{2}$;
- $\Delta^{Dynamics}_{A\rightleftarrows B} = \frac{\mathbf{N}_{AB}(t)\cdot\mathbf{v}_B(t)(t_{tx,A} - t_{tx,B} + \delta_{tx,A}(t) - \delta_{tx,B}(t) + T_{AB})}{2c}$
  $+ \frac{\mathbf{N}_{AB}(t)\cdot\mathbf{v}_A(t)(t_{tx,B} - t_{tx,A} + \delta_{tx,B}(t) - \delta_{tx,A}(t) + T_{BA})}{2c}$;
- $\Delta^{clkRate}_{A\rightleftarrows B} = \frac{\delta\dot{t}_B(t)(t_{tx,A} + t_{tx,B} + \delta_{hw,AB}(t) + T_{AB} - 2t) - \delta\dot{t}_A(t)(t_{tx,A} + t_{tx,B} + \delta_{hw,BA}(t) + T_{BA} - 2t)}{2}$;
- $\Delta^{relRate}_{A\rightleftarrows B} = \frac{\dot{\delta}_{rel,B}(t)(t_{tx,A} + t_{tx,B} + \delta_{hw,AB}(t) + T_{AB} - 2t) - \dot{\delta}_{rel,A}(t)(t_{tx,A} + t_{tx,B} + \delta_{hw,BA}(t) + T_{BA} - 2t)}{2}$;
- $\Delta^{hwRate}_{A\rightleftarrows B} = \frac{\dot{\delta}_{rx,B}(t)(t_{tx,A} + \delta_{hw,AB}(t) + T_{AB} - t) + \dot{\delta}_{tx,A}(t)(t_{tx,A} - t)}{2}$
  $- \frac{\dot{\delta}_{rx,A}(t)(t_{tx,B} + \delta_{hw,BA}(t) + T_{BA} - t) + \dot{\delta}_{tx,B}(t)(t_{tx,B} - t)}{2}$;
- $\varepsilon \sim \mathcal{N}(0, \frac{\sigma^2}{2c^2})$.

This functional model can be used to estimate the relative clock offset between the two endpoints at the common epoch t:

$$\delta\hat{t}_{AB}(t) \approx \underbrace{\Delta^{CCO}_{A\rightleftarrows B}}_{\text{Measured}} \underbrace{-\hat{\delta}_{rel,AB}(t) - \sum_i \hat{\Delta}^i_{A\rightleftarrows B}}_{\text{From model or calibration}} \tag{6}$$

where $i \in \{hw, atmo, Shapiro, Dynamics, clkRate, relRate, biasRate\}$. The terms indicated by $\hat{(\cdot)}$ are evaluated using models and calibration values.

3. Time transfer verification chain

In this section we discuss the verification of two-way time transfer (TWTT) accuracy in the context of the OpSTAR scenario. Consider a closed-loop measurement topology as the one shown in Figure 1a. At any instant t the sum of time offsets must amount to zero:

$$\delta t_{O2M2}(t) + \delta t_{M1N1}(t) + \delta t_{N2O1}(t) = 0 \tag{7}$$

Through TWTT based on the OISL and OSGLs, we obtain estimates of each offset in (7), which are affected by modeling errors from relativistic corrections, hardware delays, clock rates, relative dynamics, and atmospheric effects, plus additive measurement noise. Therefore, the sum of estimates across the loop will not equal zero as in (7), but will yield a residual error r:

$$
\begin{aligned}
r = {} & e^{rel}_{O2M2} + e^{rel}_{M1N1} + e^{rel}_{N2O1} && \text{Relativistic effects} \\
& + e^{hw}_{O2M2} + e^{hw}_{M1N1} + e^{hw}_{N2O1} && \text{Hardware delays} \\
& + e^{clk}_{O2M2} + e^{clk}_{M1N1} + e^{clk}_{N2O1} && \text{Clock instability} \\
& + e^{dyn}_{O2M2} + e^{dyn}_{M1N1} + e^{dyn}_{N2O1} && \text{Relative dynamics} \\
& + e^{atm}_{O2M2} + e^{atm}_{N2O1} && \text{Atmospheric effects} \\
& + \varepsilon_{CL} && \text{Measurement noise}
\end{aligned}
\tag{8}
$$

During mission operations, the residual term can be used as a performance indicator for time transfer via the optical links. Note that the combination of the different sources of bias, which are not necessarily all additive, might cancel out and remain unobservable. In order to mitigate this aspect, multiple measurement topologies are foreseen to be executed by exchanging terminals, satellites and OGSs linked during the same co-visibility arcs. This will be investigated in a different work. In the following, we focus on analyzing in details each potential source of error.

4. Error analysis

4.1. Simulation configuration

Let us assume to fly two satellites in trailing configuration. In order to obtain their orbits and orbit (prediction) errors, we make us of two Galileo satellites, PRN E25 and E24. As reference (true) orbits we use precise orbits from the Center for Orbit Determination in Europe, dated 1st July 2023, referenced to the satellite Center of Mass (CoM). The satellite position and velocity errors are introduced using broadcast ephemeris (BRDC) which are instead referenced to the satellite antenna phase center. However, we deliberately omit corrections from the phase center offset to CoM, emulating a larger position error with respect to the true orbits (cf. Figure 2a). We simulate only one ground station, located in Oberpfaffenhofen, Germany. A representative passage where the satellites are closest to the ground station is selected. Assuming an OSGL can be established for elevation values between 30 and 85 degrees, Figure 2b shows the ground track and co-visibility of the two satellites from the OGS.

The satellite terminal clocks are assumed to match the stability of Oven-Controlled Crystal Oscillators (OCXOs), whereas the OGS relies on a Rubidium clock. The simulated clock offset with respect to the system time is modeled as a stochastic random walk. Note that such clock model is not intended for simulation of the long-term behaviour of real clocks but allows to emulate their short term stability, the only relevant aspect for this analysis. The random walk process noise is characterized by $\sigma_{RW} = 0.8$ picoseconds per second for the OCXOs and $\sigma_{RW} = 3.5$ picoseconds per second for the Rubidium clock. Figure 2c illustrates the time evolution of the simulated clocks during a three-hour co-visibility arc.

4.2. Relativistic effects

The first relativistic term in (5), $\delta t_{rel,AB}(t)$, is the accumulated differential relativistic time offset between endpoints A and B with respect to the terrestrial reference time since the clocks' activation at $t_{A/B,init}$ till t. In the context of OpStAR this does not need to be modelled since these terms cancel out in the closed-loop:

$$\sum_{\text{closed-loop}} \delta_{rel} = \delta_{rel,M}(t) + (\delta_{rel,N}(t) - \delta_{rel,M}(t)) - \delta_{rel,N}(t) = 0 \tag{9}$$

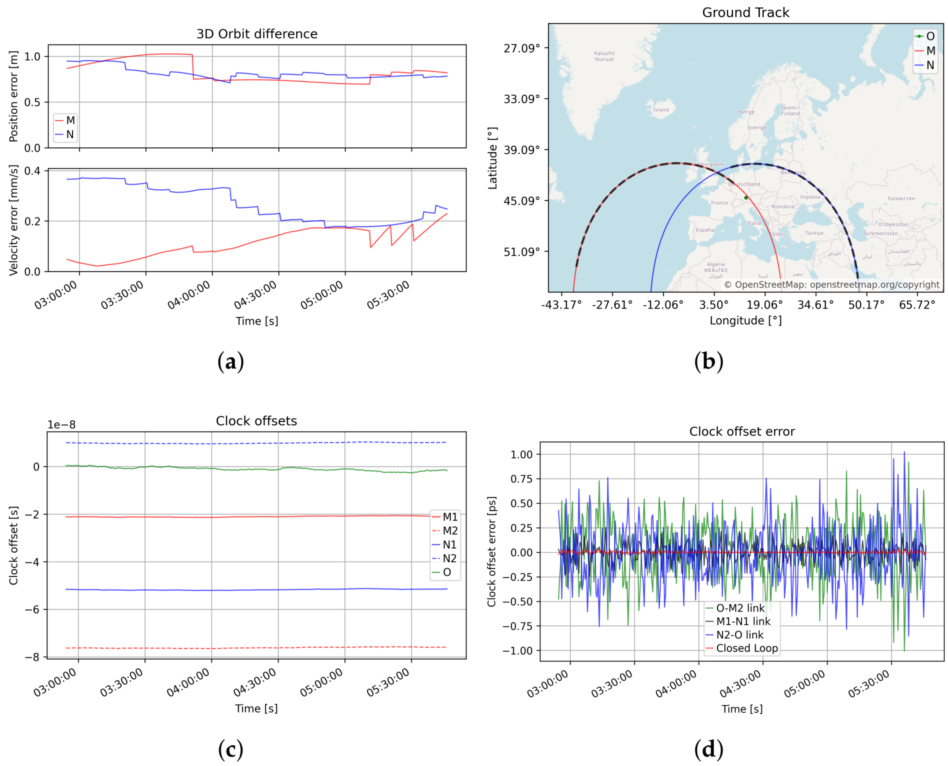

Figure 2. **(a)** Satellite orbit error as difference between precise and BRDC orbits during a 3-hour arc; **(b)** The ground track of the two satellites during the passage. The dashed lines show the parts when the satellites are mutually visible from the OGS; **(c)** The evolution of the time offset of the individual clocks; **(d)** The error due to the clocks' instability as well as the sum across the closed measurement loop. The signal emission at the endpoints A and B is assumed to be a-synchronous by $t_{tx,B} - t_{tx,A} = 0.1$ s.

The term $\Delta^{relRate}_{A\rightleftarrows B}$ is the accumulated differential relativistic time offset between endpoints A and B during the whole two-way time interval of exchange:

$$\begin{aligned}\Delta^{relRate}_{A\rightleftarrows B} &= \frac{\dot{\delta}_{rel,B}(t)(\overbrace{t_{tx,A} + \delta_{hw,AB}(t) + T_{AB}}^{\text{Reception time at B}} - t) + \dot{\delta}_{rel,B}(t)(\overbrace{t_{tx,B}}^{\text{Transmission time at B}} - t)}{2} \\ &- \frac{\dot{\delta}_{rel,A}(t)(\overbrace{t_{tx,B} + \delta_{hw,BA}(t) + T_{BA}}^{\text{Reception time at A}} - t) + \dot{\delta}_{rel,A}(t)(\overbrace{t_{tx,A}}^{\text{Transmission time at A}} - t)}{2}\end{aligned} \tag{10}$$

The term $\dot{\delta}_{rel,A/B}(t)$ is the time rate of a clock in the vicinity of Earth with respect to a terrestrial time scale and depends on the gravitational potential at the the clock's position and its velocity [5]. It is shown in [6] that errors in the satellites' position apriori knowledge of 13 meters and velocity accuracy below the centimeter per second respectively, lead to a time rate error of the order of 10^{-3} picoseconds per second. Therefore, even considering a one-second time interval for the full two-way exchange, in (10), the error on term $\Delta^{relRate}_{A\rightleftarrows B}$ remains well below the picosecond and it is thus negligible.

Finally, $\Delta^{Shapiro}_{A\rightleftarrows B}$ is the differential signal propagation relativistic delay caused by the different gravitational potential at transmit and receive points. It is shown in [6], that for TWTT based on OISLs this term is at the level of 10^{-3} picoseconds so it can also be neglected. Therefore, it can be concluded that orbits known with moderate accuracy (meter-level) no significant bias is introduced by mis-modelling relativistic effects.

4.3. Hardware delays

The terms $\Delta^{hw}_{A\rightleftarrows B}$ and $\Delta^{biasRate}_{A\rightleftarrows B}$ in (5) model the impact of differential hardware delays. If not accurately calibrated, these introduce biases and variations in the closed-loop residual r. If the hardware delays change slowly (picoseconds per second), the contribution of the term $\Delta^{biasRate}_{A\rightleftarrows B}$ becomes negligible. It should be pointed out that for TWTT verification only hardware delay differences between transmit and receive chain at the terminal is relevant. By expanding the term $\Delta^{hw}_{A\rightleftarrows B}$ one obtains:

$$\Delta^{hw}_{A\rightleftarrows B} = \frac{(\delta_{tx,A}(t) + \delta_{rx,B}(t)) - (\delta_{tx,B}(t) + \delta_{rx,A}(t))}{2} = \frac{(\delta_{tx,A}(t) - \delta_{rx,A}(t)) - (\delta_{tx,B}(t) - \delta_{rx,B}(t))}{2} \tag{11}$$

The fact that they appear as differences may lead to smaller error on the offset estimates than the error on these quantities taken individually. This shall be verified during calibration efforts on actual prototypes.

4.4. Clock stability

The contribution of clock instabilities during the TWTT exchange is expressed in term $\Delta^{clkRate}_{A\rightleftarrows B}$:

$$\Delta^{clkRate}_{A\rightleftarrows B} = \frac{\dot{\delta t}_B(t)(t_{tx,A} + \delta_{hw,AB}(t) + T_{AB} - t) + \dot{\delta t}_B(t)(t_{tx,B} - t)}{2} - \frac{\dot{\delta t}_A(t)(t_{tx,B} + \delta_{hw,BA}(t) + T_{BA} - t) + \dot{\delta t}_A(t)(t_{tx,A} - t)}{2} \tag{12}$$

As shown in Figure 2d, the contribute of clock instabilities over the TWTT exchange is mostly below picosecond-level for OCXO and Rubidium clock, even for an a-synchronous transmission at the two sides $t_{tx,B} - t_{tx,A} = 0.1$ seconds, resulting in a longer two-way exchange time. The clocks that will be procured for the OpSTAR mission are expected to provide even better short-term stability than the OCXOs considered in this study. Therefore, term $\Delta^{clkRate}_{A\rightleftarrows B}$ is negligible.

4.5. Endpoints dynamics

The relative dynamics between the two linked endpoints during the TWTT exchange is accounted in term $\Delta^{Dynamics}_{A\rightleftarrows B}$:

$$\Delta^{Dynamics}_{A\rightleftarrows B} = \frac{\mathbf{N}_{AB}(t) \cdot \mathbf{v}_B(t)(t_{tx,A} - t_{tx,B} + \delta_{tx,A}(t) - \delta_{tx,B}(t) + T_{AB})}{2c} + \frac{\mathbf{N}_{AB}(t) \cdot \mathbf{v}_A(t)(t_{tx,B} - t_{tx,A} + \delta_{tx,B}(t) - \delta_{tx,A}(t) + T_{BA})}{2c} \tag{13}$$

This term can be computed with the estimated satellite positions and velocities obtained from orbit determination/prediction. In order to assess the impact of relative dynamics, the correction $\Delta^{Dynamics}_{A\rightleftarrows B}$ term is computed over one passage using both precise orbits (used as ground truth) and predicted BRDC orbits, for different values of transmission a-synchronicity ($t_{tx,B} - t_{tx,A}$), ranging from 10^{-5} to 1 second. The hardware delays are here neglected. Table 1 reports model errors (absolute values) for the individual links and for their cumulative closed-loop sum.

The results show that even with large transmission a-synchronicity (1 second) and significant satellite position errors (meter-level, cf. Figure 2a), synchronization errors remain below the picosecond-level. Note that the total contribution of each error in the closed-loop is smaller than the sum of the single components.

Table 1. Error in the determination of correction $\Delta_{A\rightleftarrows B}^{Dynamics}$ using BRDC orbits instead of precise ones.

Transmit a-synchronicity $t_{tx,B} - t_{tx,A}$ [s]	Max/Avg correction error [ps] M1 - N1	O1 - M2	O2 - N2	O1 - M2 - M1 - N1 - N2 - O2
10^{-5}	0.06/0.03	0.03/0.02	0.04/0.02	0.08/0.03
0.1	0.07/0.03	0.01/0.00	0.01/0.01	0.05/0.02
1	0.36/0.15	0.23/0.12	0.45/0.26	0.44/0.18

4.6. Atmospheric delays

The last term in (3) is the differential atmospheric delay:

$$\Delta_{A\rightleftarrows B}^{atmo} = \frac{\delta T_{AB,atmo}(t_{tx,A}, T_{AB}) - \delta T_{BA,atmo}(t_{tx,B}, T_{BA})}{2} \tag{14}$$

Available atmospheric models [5] are characterized by an overall root mean square error for the total zenith delay below 1 millimeter across the optical spectrum between 355 and 1064 nanometers wavelengths. Lower elevations increase this value, and modeling errors might increase according to the accuracy of the mapping function used. However, the differential atmospheric delay might largely mitigate the impact of any mis-modeling during the two-way exchange, due to the slow spatial and temporal variations of the medium properties. Further investigations are necessary to quantitatively assess the impact of atmospheric effects in TWTT via optical links.

4.7. Noise

The optical terminals being designed for the OpSTAR mission target sub-picosecond precision in the generation of time stamps. The overall pseudorange measurement precision will be impacted by additional sources of noise, such as frequency reference jitter, electronic components, cables propagation, platform vibrations, mechanical actuators for the optical heads, as well as additional contributions during free-space propagation. While an overall analysis of the precision of TWTT observables can only be performed during an actual mission, preliminary tests conducted by DLR provided an insight on the performance achievable in a free-space optical link testbed. In this experiment, optical transceivers (breadboards) have been used to test TWTT over a 10.45 kilometers free-space optical link, effectively emulating the atmospheric path experienced by a space-to-ground link between a GEO satellite and a ground station at 2 degrees of elevation. The experiment showed TWTT observables at sub-picosecond stability (Allan Deviation at 1 second) [3,7]. Further assessment on the measurement noise will be performed in the context of the OpSTAR mission.

5. Conclusions

A verification chain based on a closed-loop topology of links is proposed as indicator of accuracy of TWTT via OISLs and OSGLs. By analysing the residuals of the sum of the clock offset estimates across the loop it is possible to identify potential unwanted bias sources. The analyses presented in this work show that the impact of relativistic effects, high relative dynamic, and clock instabilities do not present any difficulty in the modeling of optical observables. By contrast, the impact of hardware and atmospheric delays necessitates of further investigations during the preparation phases and execution of the planned OpSTAR in-orbit demonstrator.

It is essential to note that sub-picosecond residuals in the sum of errors within the closed-loop does not necessarily guarantee individual link accuracy. Conversely, any "common" error in the individual links with a opposite sign will cancel out, potentially masking unobservable biases. To address this limitation, alternative closed-loop topologies could be employed to improve bias identification: this is a topic of future research.

Author Contributions: Conceptualization, M.D. and G.G.; methodology, software, writing, M.D.; writing—review, M.D. and G.M. and G.G.; supervision, project administration, funding acquisition, G.G. All authors have read and agreed to the published version of the manuscript.

Funding: This research was carried in the framework of the OpSTAR-AB study, an ESA-led Navisp Element 3 activity.

Data Availability Statement: The original data presented in the study are openly available in the Crustal Dynamics Data Information System (CDDIS) at [8]. Map data are sourced from OpenStreetMap, openstreetmap.org/copyright.

Conflicts of Interest: The authors declare no conflicts of interest.

Abbreviations

CCO	Cross-link Clock Observable
CoM	Center of Mass
DLR	Deutsches Zentrum für Luft- und Raumfahrt (German Aerospace Center)
OCXO	Oven-Controlled Crystal Oscillator
OGS	Optical Ground Station
OISL	Optical Inter-Satellite Link
OSGL	Optical Satellite-to-Ground Link
OpSTAR	Optical Synchronized Time And Ranging
TWTT	Two-Way Time Transfer

References

1. Meng, W.; Zhang, H.; Huang, P.; Wang, J.; Zhang, Z.; Liao, Y.; Ye, Y.; Hu, W.; Wang, Y.; Chen, W.; et al. Design and experiment of onboard laser time transfer in chinese beidou navigation satellites. *Advances in Space Research* **2013**, *51*, 951–958. https://doi.org/10.1016/j.asr.2012.08.007.
2. Exertier, P.; Samain, E.; Martin, N.; Courde, C.; Laas-Bourez, M.; Foussard, C.; Guillemot, P. Time Transfer by Laser Link: Data analysis and validation to the ps level. *Advances in Space Research* **2014**, *54*, 2371–2385. https://doi.org/https://doi.org/10.1016/j.asr.2014.08.015.
3. Surof, J.; Poliak, J.; Wolf, R.; Macri, L.; Mata Calvo, R.; Blümel, L.; Dominguez, P.N.; Giorgi, G.; Agazzi, L.; Furthner, J.; et al. Validation of Kepler Time and Frequency Transfer on a Terrestrial Range of 10.45km. In Proceedings of the ION GNNS+, September 2022, Proceedings of the 35th International Technical Meeting of the Satellite Division of The Institute of Navigation (ION GNSS+ 2022), pp. 3662–3670.
4. Fernández, F.A. Inter-satellite ranging and inter-satellite communication links for enhancing GNSS satellite broadcast navigation data. *Advances in Space Research* **2011**, *47*, 786–801. https://doi.org/10.1016/j.asr.2010.10.002.
5. Petit, G.; Luzum, B. IERS Conventions (2010) - IERS Technical Note 36. Technical report, Observatoire de Paris, 2010. https://doi.org/ISBN3-89888-989-6.
6. Dassié, M.; Giorgi, G. Relativistic Modelling for Accurate Time Transfer via Optical Inter-Satellite Links. *Aerotecnica Missili & Spazio* **2021**. https://doi.org/10.1007/s42496-021-00087-1.
7. Giggenbach, D.; Poliak, J.; Mata-Calvo, R.; Fuchs, C.; Perlot, N.; Freund, R.; Richter, T. Preliminary Results of Terabit-per-second Long-Range Free-Space Optical Transmission Experiment THRUST. In Proceedings of the Advanced Free-Space Optical Communication Techniques and Applications; Laycock, L.; White, H.J., Eds. SPIE Press, October 2015, number 9647B.
8. Noll, C. The Crustal Dynamics Data Information System: A resource to support scientific analysis using space geodesy. *Advances in Space Research* **2010**, *45*, 1421–1440. https://doi.org/10.1016/j.asr.2010.01.018.